nature neuroscience

Glutamate exocytosis from astrocytes controls synaptic strength

Pascal Jourdain[1,6], Linda H Bergersen[2,6], Khaleel Bhaukaurally[1,6], Paola Bezzi[1], Mirko Santello[1], Maria Domercq[3], Carlos Matute[3], Fiorella Tonello[4], Vidar Gundersen[2,5] & Andrea Volterra[1]

The release of transmitters from glia influences synaptic functions. The modalities and physiological functions of glial release are poorly understood. Here we show that glutamate exocytosis from astrocytes of the rat hippocampal dentate molecular layer enhances synaptic strength at excitatory synapses between perforant path afferents and granule cells. The effect is mediated by ifenprodil-sensitive NMDA ionotropic glutamate receptors and involves an increase of transmitter release at the synapse. Correspondingly, we identify NMDA receptor 2B subunits on the extrasynaptic portion of excitatory nerve terminals. The receptor distribution is spatially related to glutamate-containing synaptic-like microvesicles in the apposed astrocytic processes. This glial regulatory pathway is endogenously activated by neuronal activity–dependent stimulation of purinergic P2Y1 receptors on the astrocytes. Thus, we provide the first combined functional and ultrastructural evidence for a physiological control of synaptic activity via exocytosis of glutamate from astrocytes.

Brain communication via vesicular exocytosis and quantal release of transmitter has long been considered to be specific to neuronal synapses. There is strong evidence, however, that astrocytes release transmitters, such as glutamate, through a Ca^{2+}-regulated mechanism[1–5]. Recently, the direct observation of exocytic fusions of glutamatergic vesicles in cultured astrocytes[6–8] and the ultrastructural identification of synaptic-like microvesicles (SLMVs) equipped with the machinery for storing and releasing glutamate in astrocytes of the adult hippocampus[6,9,10] have considerably substantiated the evidence for an exocytotic pathway of glutamate release from astrocytes.

Astrocytes *in situ* respond to synaptically released neurotransmitters and other signaling substances with intracellular Ca^{2+} ($[Ca^{2+}]_i$) elevations that may, in turn, activate the astrocytes to release glutamate[10]. Synaptic glutamate triggers its own release from astrocytes by stimulating astrocytic metabotropic glutamate receptors (mGluRs)[2,6,11]. ATP, released from neurons or astrocytes during synaptic activity, induces $[Ca^{2+}]_i$ elevations mediated by G protein–coupled purinergic receptors of the P2Y1 type (P2Y1Rs) in hippocampal astrocytes[12]. We recently found that P2Y1R signaling in astrocytes is coupled to Ca^{2+}-dependent glutamate exocytosis[7].

Together, the above data strongly suggest that a bidirectional neuron-astrocyte communication involving exocytosis of glutamate from astrocytes exists *in vivo*. However, the occurrence of this phenomenon is not fully documented and no information exists about the structural-functional relationships that would govern it. Consequently, its physiological significance remains unknown.

To address these questions, we studied communication between astrocytes in the hippocampal dentate molecular layer and excitatory synapses on dentate granule cells using a combination of patch-clamp electrophysiology, Ca^{2+} imaging and high-resolution immunogold cytochemistry. We show that glutamate exocytosis from astrocytes enhances synaptic strength at these synapses. The effect is mediated via presynaptic NMDA ionotropic glutamate receptor 2B subunit (NR2B)-containing NMDA receptors (NMDARs) that increase the probability of transmitter release at the synapse. We consistently identified NR2B subunits on the extrasynaptic portion of excitatory nerve terminals making synapses on granule cell spines, mostly lying within synaptic distance from SLMVs in the facing astrocytic processes. The astrocytic control is endogenously activated by activity-dependent stimulation of astrocytic purinergic P2Y1Rs during normal functioning of these synapses.

RESULTS

Astrocyte-induced synaptic potentiation

We took dual whole-cell patch-clamp recordings from cell pairs consisting of a molecular layer astrocyte and a dentate granule cell in rat hemibrain horizontal slices, bathed in Mg^{2+}-containing medium with the $GABA_A$ receptor blocker picrotoxin added. This approach allowed us to stimulate the astrocyte selectively and to perfuse it internally with agents preventing exocytosis, while simultaneously monitoring excitatory activity in the granule cell (see Methods). In each experiment, we initially verified the electrical properties of the

[1]Department of Cell Biology and Morphology, University of Lausanne, Rue du Bugnon 9, 1005 Lausanne, Switzerland. [2]Department of Anatomy and the Centre of Molecular Biology and Neuroscience, University of Oslo, POB 1105 Blindern, 0317 Oslo, Norway. [3]Department of Neurosciences, University of the Basque Country, 48640 Leioa, Vizcaya, Spain. [4]Department of Biomedical Sciences, University of Padova, Viale Colombo, 3, 35121 Padova, Italy. [5]Department of Neurology, Rikshospitalet University Hospital, 0023 Oslo, Norway. [6]These authors contributed equally to this work. Correspondence should be addressed to A.V. (andrea.volterra@unil.ch) or to V.G. (vidar.gundersen@medisin.uio.no).

Received 29 September 2006; accepted 16 January 2007; published online 18 February 2007; doi:10.1038/nn1849

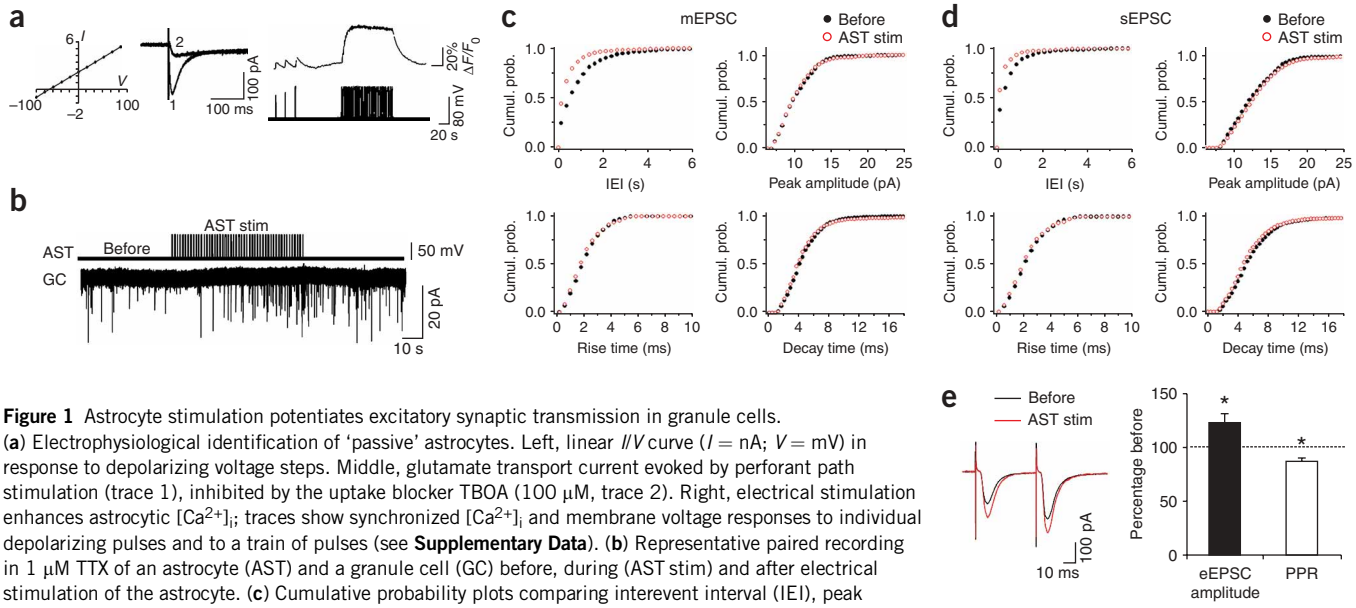

Figure 1 Astrocyte stimulation potentiates excitatory synaptic transmission in granule cells. (**a**) Electrophysiological identification of 'passive' astrocytes. Left, linear *I*/*V* curve (*I* = nA; *V* = mV) in response to depolarizing voltage steps. Middle, glutamate transport current evoked by perforant path stimulation (trace 1), inhibited by the uptake blocker TBOA (100 μM, trace 2). Right, electrical stimulation enhances astrocytic $[Ca^{2+}]_i$; traces show synchronized $[Ca^{2+}]_i$ and membrane voltage responses to individual depolarizing pulses and to a train of pulses (see **Supplementary Data**). (**b**) Representative paired recording in 1 μM TTX of an astrocyte (AST) and a granule cell (GC) before, during (AST stim) and after electrical stimulation of the astrocyte. (**c**) Cumulative probability plots comparing interevent interval (IEI), peak amplitude, rise time and decay time (bins, 0.25 s, 0.5 pA, 0.4 ms, 0.4 ms, respectively) of mEPSCs in granule cells before (black dots) and during astrocyte stimulation (red open dots). Stimulation selectively modifies mEPSC frequency ($P < 0.001$, KS test). (**d**) Analogous plots for sEPSC activity. KS test indicates a selective effect on frequency ($P < 0.001$). (**e**) Left, representative paired-pulse EPSCs evoked in a granule cell by perforant path stimulation before (black traces) and immediately after (red traces) astrocyte stimulation. Right, eEPSC amplitude (first eEPSC of a paired-pulse, black histogram) and PPR (white histogram) after astrocyte stimulation, expressed as the percentage of the values before stimulation (absolute values before stimulation: eEPSC amplitude, –166 ± 33 pA; PPR, 1.36 ± 0.19; after stimulation: eEPSC amplitude, –193 ± 35 pA; PPR, 1.25 ± 0.2; $^*P < 0.05$ versus before, paired *t*-test).

patched astrocyte and then only further studied those showing 'passive' properties[13], as they correspond to the astrocytic population containing glutamatergic SLMVs[6]. These cells ($n = 29$) had a linear current-voltage relationship, highly negative resting potential (–82 ± 6 mV) and low input resistance (14 ± 5 MΩ), and responded to stimulation of perforant path afferent fibers with glutamate uptake currents that are blocked by the glutamate transporter inhibitor DL-*threo*-β-benzyloxy-aspartic acid[14] (TBOA; **Fig. 1a**).

In parallel, we recorded neuronal activity in granule cells. Before stimulation of the astrocyte, such activity consisted of spontaneous transient inward currents with fast kinetics typical of synaptic events (rise time: 2.65 ± 0.25 ms, mean ± s.e.m.; range, 0.58–6.40 ms; decay time: 5.53 ± 0.35 ms, range, 2.10–29.66 ms), a mean amplitude of 13.41 ± 1.08 pA, and a frequency of 1.62 ± 0.30 Hz ($n = 15$ cells). Spontaneous excitatory postsynaptic currents (sEPSCs) were abolished by the AMPA/kainate receptor blocker 1,2,3,4-tetrahydro-6-nitro-2,3-dioxo-benzo[*f*]quinoxaline-7-sulfonamide (NBQX, 20 μM). To stimulate the patched astrocyte, we applied a train of depolarizing pulses through the patch pipette[15] (see Methods, **Supplementary Table 1** online and **Supplementary Fig. 1** online). Despite inducing a nonphysiological electrical response, this protocol triggers a physiologically relevant chemical response in the astrocyte, consisting of a reversible $[Ca^{2+}]_i$ elevation from internal Ca^{2+} stores (**Fig. 1a** and **Supplementary Data** online), followed by glutamate release[15]. In 5 out of 15 recorded pairs, stimulation of the astrocyte increased sEPSC frequency in the granule cell (from 1.61 ± 0.23 Hz to 2.64 ± 0.34 Hz; $P < 0.05$). The effect reached statistical significance 41 ± 10 s (range, 15–65 s) after the start of stimulation and was not accompanied by changes in sEPSC amplitude (before stimulation: 13.35 ± 1.91 pA; after stimulation: 12.84 ± 1.55 pA) and kinetics (before stimulation: rise time, 2.30 ± 0.33 ms, decay time, 5.46 ± 0.40 ms; after stimulation: rise time, 2.57 ± 0.23 ms, decay time, 6.12 ± 0.36 ms; **Fig. 1d**). The effect was astrocyte specific, because application of an identical stimulation protocol to the surrounding neuropil never modified sEPSC activity in granule cells (**Supplementary Fig. 2** online). In the remaining ten pairs, stimulation of the astrocyte did not affect activity in the selected granule cell, suggesting that any molecular layer astrocyte sends functional inputs to about one-third of the surrounding synapses on granule cells.

We then repeated experiments in the presence of tetrodotoxin (TTX) to block action potential–dependent neuronal activity (**Fig. 1b**,**c**). The mean amplitude and frequency of the miniature events (mEPSCs) were 78% and 58%, respectively, of those of the sEPSCs ($n = 14$ cells). Nonetheless, in 5 out of 14 pairs with TTX, stimulation of the astrocyte significantly enhanced the frequency of mEPSCs in the granule cell (from 0.9 ± 0.1 Hz to 1.72 ± 0.28 Hz; $P < 0.05$ within 40 ± 12 s from the start of astrocyte stimulation), without changing their amplitude, rise or decay time (before stimulation: 10.50 ± 1.14 pA, 2.31 ± 0.31 ms, 4.96 ± 0.40 ms, respectively; after stimulation: 10.35 ± 1.06 pA, 2.12 ± 0.2 ms, 4.65 ± 0.24 ms, respectively). Overall, the effects on sEPSCs and mEPSCs indicate that astrocyte stimulation potentiates the presynaptic input to granule cells. The selective increment of mEPSC frequency suggests a facilitating action at the level of presynaptic terminals.

To test whether the astrocytic input causes an overall strengthening of synaptic connectivity, we stimulated astrocytes while evoking EPSCs (eEPSCs) in granule cells by stimulation of perforant path afferents (see Methods). Astrocyte stimulation increased eEPSC amplitude in 7 out of 19 pairs, whereas it produced no changes in the other pairs (**Fig. 1e**). The potentiating effect was accompanied by a modified paired-pulse ratio (PPR) of the eEPSCs, suggesting that stimulation of molecular layer astrocytes increases the probability of presynaptic transmitter release at perforant path–granule cell synapses.

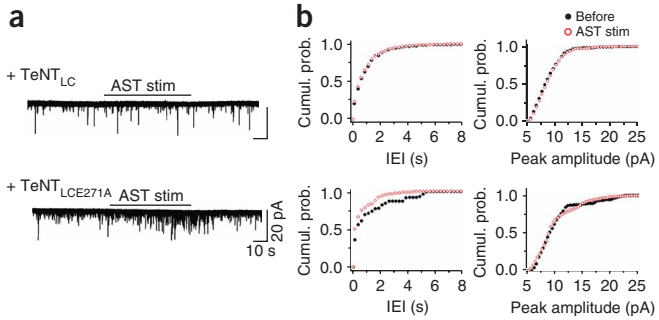

Figure 2 Blockade of exocytosis in astrocytes prevents the astrocyte-evoked enhancement of mEPSC frequency in granule cells. (**a**) Representative traces of mEPSC activity in granule cells. Astrocyte stimulation does not modify mEPSC frequency if the astrocyte contains active TeNT$_{LC}$ (upper), whereas it increases frequency if it contains inactive TeNT$_{LCE271A}$ (lower). (**b**) Cumulative probability plots of mEPSC frequency (expressed as IEI; bin, 0.25 s, left) and amplitude (bin, 0.5 pA, right) before and during stimulation of astrocytes containing TeNT$_{LC}$ (upper, data from all the patched granule cells) or TeNT$_{LCE271A}$ (lower, data from the three responding granule cells; IEI, $P < 0.05$ versus before stimulation, KS test).

Blocking exocytosis in astrocytes prevents potentiation

We then tested whether astrocyte-dependent synaptic potentiation requires exocytosis of an astrocytic transmitter. While patching astrocyte–granule cell pairs, we introduced the active light-chain of tetanus neurotoxin (TeNT$_{LC}$) into the astrocyte. TeNT$_{LC}$ selectively cleaves and inactivates the vesicle-associated membrane protein (VAMP), which is an indispensable component of the SNARE fusion complex. Consequently, TeNT specifically blocks exocytosis of synaptic vesicles[16]. Moreover, it prevents fusion of glutamatergic vesicles in cultured astrocytes[6,7]. Appropriate conditions for these experiments were set in separate tests. We estimated the time needed (10 min) for TeNT$_{LC}$ to diffuse into the distal processes of the patched astrocyte using a fluorescent molecule of equal molecular weight (dextran 40000–fluorescein), and the toxin concentration (120 nm) to be introduced in the astrocyte by checking the cleavage of VAMP in astrocytic membrane fractions exposed to TeNT$_{LC}$ (data not shown). In 11 TeNT$_{LC}$ experiments, stimulation of the astrocyte never enhanced mEPSC frequency in the granule cell (**Fig. 2a**,**b**, top). To ascertain the specificity of the inhibitory effect of TeNT$_{LC}$, we used TeNT$_{LCE271A}$ as a control. TeNT$_{LCE271A}$ contains a single-amino-acid mutation at the active site, which abolishes the toxin's capacity to cleave VAMP[17]. In the presence of TeNT$_{LCE271A}$, stimulation of the astrocyte enhanced mEPSC frequency (**Fig. 2a**,**b**, bottom) in three out of nine astrocyte–granule cell pairs (that is, the same proportion as without TeNT). Therefore, the mechanism underlying astrocytic potentiation of granule cell synapses is TeNT sensitive and requires SNARE-dependent vesicle fusion.

Potentiation is mediated by NR2B-containing NMDARs

We previously observed that glutamatergic SLMVs in astrocytic processes are often opposite to neuronal structures expressing NMDAR subunits[6]. Therefore, we tested whether NMDARs mediate the astrocytic synaptic control. In 13 cell pairs, stimulation of the astrocyte in the presence of the NMDAR antagonist D-(–)-2-amino-5-phosphonopentanoic acid (AP5) never modified mEPSC frequency in the granule cell (**Fig. 3b**). After AP5 washout, however, the same stimulation significantly enhanced mEPSC frequency in 4 of the 13 granule cells without affecting mEPSC amplitude (**Supplementary Fig. 3** online). The NR2B-selective NMDAR antagonist ifenprodil reproduced the effect of AP5 (**Fig. 3a**,**b**): in its presence, stimulation of the astrocyte never increased mEPSC frequency in the granule cell ($n = 11$ cell pairs), whereas after ifenprodil washout it did so in 4 of the 11 granule cells, again without changing mEPSC amplitude (**Supplementary Fig. 3**).

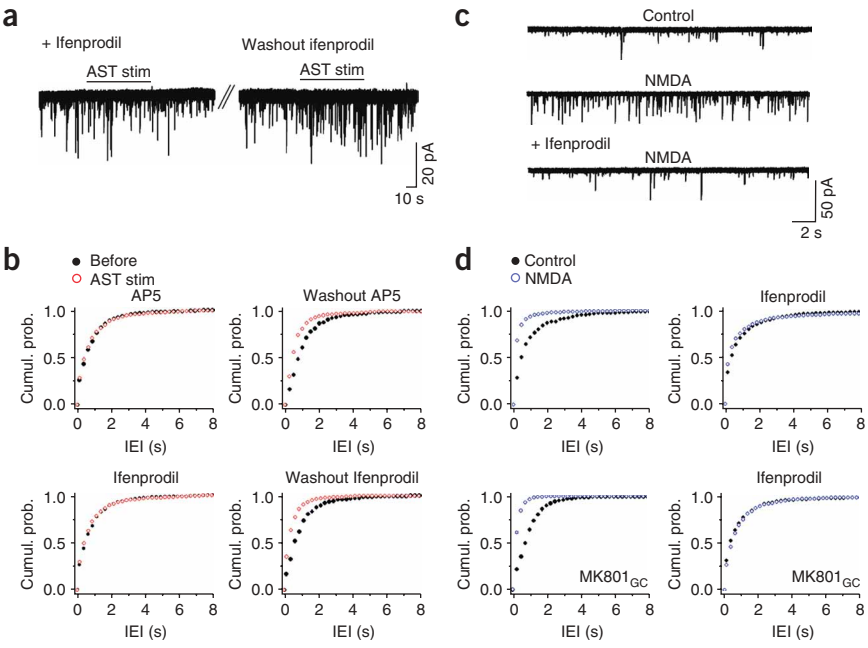

Figure 3 NR2B-containing NMDARs mediate the enhancement of mEPSC frequency in granule cells. (**a**) Representative recordings in a granule cell showing the effect of astrocyte stimulation on mEPSC activity in the presence of the NR2B-selective NMDAR antagonist ifenprodil (3 μM, left) and after its washout (right). (**b**) Cumulative probability plots comparing mEPSC frequency changes (expressed as IEI; bin, 0.25 s) induced in responding granule cells by astrocyte stimulation in the presence of an NMDAR antagonist, either 50 μM AP5 or 3 μM ifenprodil (left), and after its washout (right). Significant changes are seen only after washout of the NMDAR antagonist ($P < 0.001$ in both experiments with AP5 and ifenprodil, KS test). Corresponding plots of mEPSC amplitude are shown in **Supplementary Figure 3**. (**c**) NMDA mimics the effect of astrocyte stimulation. The traces show mEPSC events in a granule cell before NMDA application (control), during application (NMDA, 5 μM) and when NMDA is applied in the presence of ifenprodil (3 μM). The granule cell is voltage clamped at –80 mV. (**d**) Cumulative probability plots showing, left, effect of NMDA on mEPSC frequency (expressed as IEI; bin, 0.25 s) in granule cells without the NMDA channel blocker MK801 (top, $P < 0.001$) or with MK801 (bottom, 2 mM, MK801$_{GC}$, $P < 0.001$; see also **Supplementary Fig. 4**); right, blockade of the NMDA effect by ifenprodil. Top, granule cells without MK801; bottom, granule cells with MK-801. Statistical analysis was performed with KS test. Corresponding plots of mEPSC amplitude are shown in **Supplementary Figure 3**.

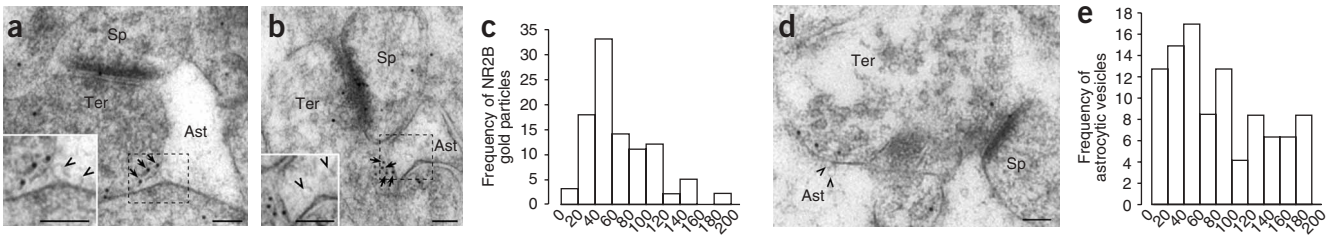

Figure 4 NR2B in extrasynaptic terminal membranes is close to SLMVs in apposed astrocytic processes, and SLMVs are close to the astrocytic plasma membranes that face NR2B. (**a**,**b**) Electron micrographs showing NR2B gold particles in extrasynaptic membranes (arrows) of nerve terminals (Ter) making asymmetric synapses with dendritic spines (Sp) in the dentate molecular layer. NR2B particles face astrocytic processes (Ast) that contain SLMVs. NR2B is in close proximity to astrocytic SLMVs. Insets, higher magnification showing NR2B gold particles and astrocytic SLMVs (arrowheads). Scale bars, 100 nm. (**c**) Analysis of the distance from each NR2B gold particle to the closest astrocytic SLMV. The distances were sorted into bins of 20 nm (*x* axis). (**d**). Electron micrograph taken in the dentate molecular layer showing that SLMVs are located close to the astrocytic plasma membrane. The astrocytic process apposed to the terminal contains SLMVs, of which two (arrowheads) are closely attached to the plasma membrane. The NR2B gold particles in the nerve terminal are located within about 30 nm of the plasma membrane, implying that they may signal receptors in this membrane[49] (Sp, dendritic spine). Scale bar, 100 nm. (**e**) Frequency histogram showing the distribution of SLMVs in astrocytic processes facing terminals forming asymmetric synapses on spines in the dentate molecular layer. The distance (nm) between the vesicles and the astrocytic plasma membrane was recorded for all vesicles situated within 200 nm. The distances were put into bins of 20 nm and their frequency distribution calculated.

The reversed protocol gave an identical result. In two cell pairs where astrocyte stimulation enhanced mEPSC frequency, the effect was subsequently abolished when we repeated stimulation in the presence of ifenprodil. In addition, ifenprodil prevented the astrocyte-induced potentiation of eEPSCs (percentage increase in eEPSC amplitude after astrocyte stimulation versus before: with ifenprodil, 2 ± 3%; after ifenprodil washout, 26 ± 2%; $n = 7$; see Methods). Therefore, the astrocyte-dependent effect requires activation of NMDARs containing the NR2B subunit.

To establish whether activation of such receptors is not only necessary but also sufficient to induce synaptic strengthening, we applied NMDA in the presence of TTX and recorded current responses from granule cells voltage-clamped at –80 mV, without patching the astrocytes. NMDA increased the number of mEPSC events by threefold (**Fig. 3c**,**d**; $n = 7$) without changing their mean amplitude (**Supplementary Fig. 3**). Ifenprodil fully prevented the NMDA-dependent enhancement (**Fig. 3c**,**d** and **Supplementary Fig. 3**; $n = 4$), indicating that NMDA acts selectively via NR2B-containing receptors. In another set of experiments (**Fig. 3d**, bottom, and **Supplementary Figs. 3** and **4** online), we internally perfused the patched granule cell with the NMDA channel blocker MK-801. By using conditions that favor open-channel blockade, we effectively abolished NMDAR-dependent currents in the granule cell. Nonetheless, in six out of six granule cells containing MK801, the ifenprodil-sensitive NMDA effect on mEPSCs persisted. We further considered the possible involvement of extrasynaptic NR2B-containing receptors, as in CA1 pyramidal neurons these receptors are activated by glutamate released from astrocytes and mediate characteristic ifenprodil-sensitive slow inward currents (SICs)[18]. We adopted the same identification criteria for SICs used in CA1 pyramidal cells[19] (see Methods), but in our experimental conditions we did not detect this type of current events in dentate granule cells undergoing astrocyte-dependent synaptic potentiation. SICs were, however, sometimes observed during recordings in Mg^{2+}-free medium (**Supplementary Table 2** online). Altogether, the above observations strongly suggest a presynaptic localization of the relevant NR2B-containing NMDA receptors.

NR2B is in nerve terminals synapsing on granule cell spines

Postembedding immunogold cytochemistry gave independent evidence for this notion. We found NR2B gold particles at excitatory synapses on granule cell spines in both synaptic and extrasynaptic locations and, in the latter, on plasma membranes of both spines and nerve terminals (**Fig. 4**). In addition, they were associated with vesicular organelles in the nerve terminals, suggesting that NR2B subunits are trafficked to and from the plasma membrane. Focusing on the extrasynaptic neuronal membranes facing astrocytes, we found NR2B gold particles preponderantly associated with the terminal membranes (**Fig. 4a**,**b**), with a cross-membrane distribution that corresponded to that of proteins inserted in the plasma membrane (**Supplementary Fig. 5** online). Twenty-eight percent of extrasynaptic terminal membrane profiles carried NR2B gold particles, twice the percentage of NR2B-positive extrasynaptic dendritic membrane profiles (13.5%; $n = 87$ synapses). The total number of NR2B gold particles along extrasynaptic terminal membranes directly facing astrocytic membranes exceeded the number along extrasynaptic dendritic membranes facing astrocyte membranes by fourfold, suggesting a prevailing presynaptic distribution.

Astrocytic vesicles colocalize with presynaptic NR2B

In parallel, we studied the distribution of SLMVs in the astrocytic processes surrounding the excitatory synapses. We found that 39% of the profiles of astrocytic processes facing neuronal structures contained SLMVs ($n = 30$ synapses). The average density of these vesicles was 20.6 ± 8.0 vesicles per μm^2 (mean ± s.d.), about ninefold lower than that observed in adjacent nerve terminals. A large proportion were in close proximity to the astrocytic plasma membrane, and about 13% had their center within 20 nm of the membrane (**Fig. 4d**,**e**), indicating the presence of 'docked' vesicles in the astrocytic processes. The total number of astrocytic SLMVs was 3.5-fold higher in processes facing terminals than in those facing dendrites. Notably, by using specific antibodies to glutamate, we estimated that the astrocytic SLMVs contained approximately the same concentrations of glutamate as did the synaptic vesicles of adjacent excitatory nerve terminals (mean number of glutamate immunogold particles per μm^2 ± s.d. in SLMVs and synaptic vesicles: 642 ± 269, $n = 44$ astrocytic processes, and 757 ± 266, $n = 13$ nerve terminals) and severalfold higher than the corresponding cytosolic levels (L.H.B., A.V. and V.G., unpublished data).

Next, we asked whether the distributions of glutamatergic SLMVs in astrocytes and NR2B in nerve terminals are associated. After measuring the distance from the center of each NR2B-signaling gold particle

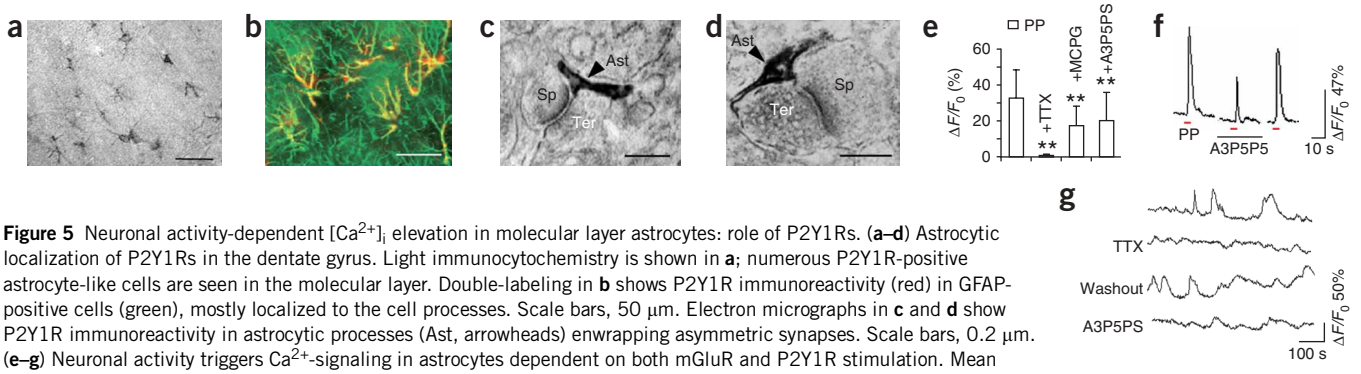

Figure 5 Neuronal activity-dependent $[Ca^{2+}]_i$ elevation in molecular layer astrocytes: role of P2Y1Rs. (**a–d**) Astrocytic localization of P2Y1Rs in the dentate gyrus. Light immunocytochemistry is shown in **a**; numerous P2Y1R-positive astrocyte-like cells are seen in the molecular layer. Double-labeling in **b** shows P2Y1R immunoreactivity (red) in GFAP-positive cells (green), mostly localized to the cell processes. Scale bars, 50 μm. Electron micrographs in **c** and **d** show P2Y1R immunoreactivity in astrocytic processes (Ast, arrowheads) enwrapping asymmetric synapses. Scale bars, 0.2 μm. (**e–g**) Neuronal activity triggers Ca^{2+}-signaling in astrocytes dependent on both mGluR and P2Y1R stimulation. Mean astrocytic Ca^{2+} responses to stimulation of perforant path fibers in control condition and in the presence of TTX (1 μM), MCPG (500 μM) or A3P5PS (100 μM) are shown in **e**. Data (± s.e.m.) are expressed as $\Delta F/F_0$ at the peak of the response; ** $P < 0.01$ versus control, one-way ANOVA and Scheffé test. Representative Ca^{2+} transients evoked in an astrocyte by stimulation of perforant path afferents (red dashes) applied first in control condition (left), then in the presence of A3P5PS (100 μM, center) and finally after washout of the drug (right) are shown in **f**. Representative traces are shown in **g** of endogenous $[Ca^{2+}]_i$ activity in an astrocyte recorded sequentially in (top to bottom): control condition, with TTX present, after TTX washout, and with A3P5PS present.

($n = 75$) in the extrasynaptic part of the terminal plasma membrane to the center of the closest SLMV in an astrocytic process, we found that 75% of the gold particles had an astrocytic vesicle within 200 nm. The majority (68%) of the latter was located closer than 100 nm to a vesicle and 33% were between 40 and 60 nm (**Fig. 4c**).

Activity-dependent astrocyte signaling via P2Y1Rs

We next investigated whether glutamate exocytosis from astrocytes participates in the physiological control of synaptic strength. We have recently identified purinergic P2Y1Rs as an endogenous signaling system coupled to glutamate exocytosis in astrocytes, but not in neurons[7]. The same receptors mediate ATP-dependent activation of astrocytes in response to nerve afferent stimulation in the CA1 hippocampal region[12]. On the basis of this information, we decided to study the distribution of P2Y1Rs in the dentate gyrus with specific antibodies[20] (**Fig. 5a–d**). P2Y1R-positive cells were localized in the molecular layer, showed astrocytic morphology and were double-labeled by the astrocytic marker glial fibrillary acidic protein (GFAP). At the ultrastructural level, P2Y1R-positive profiles were identified as astrocytic processes surrounding asymmetric synapses on granule cell spines. Forty-three percent of such synapses (an underestimate of the actual proportion, see **Supplementary Note** online; $n = 190$) showed perisynaptic astrocytic P2Y1R immunoreactivity. We therefore tested whether astrocytic P2Y1Rs are activated during synaptic transmission at granule cell synapses. In 14 slices, stimulation of perforant path afferents consistently induced transient $[Ca^{2+}]_i$ elevations in several astrocyte-like cells of the molecular layer ($n = 162$ cells; **Fig. 5e,f**). These cells were all double-labeled by sulforhodamine-101 (SR101), a dye reported to stain astrocytes selectively[21]. Ten of them were randomly selected and patched at the end of the experiments, and all of them displayed 'passive' astrocyte properties. In ten of the above slices, we repeated stimulation in the presence of TTX. None of the previously responding astrocytes underwent $[Ca^{2+}]_i$ elevation ($n = 111$ cells; **Fig. 5d**), demonstrating that they responded to the firing activity of perforant path fibers. $[Ca^{2+}]_i$ increases were also significantly inhibited by the mGluR antagonist (*S*)-α-methyl-4-carboxyphenylglycine (MCPG; $n = 48$ cells in four of the above slices) and unexpectedly, by the selective P2Y1R antagonist adenosine-3-phosphate-5-phosphosulfate[22] (A3P5PS; $n = 80$ cells in eight of the above slices; **Fig. 5e,f**). Therefore, P2Y1Rs, together with mGluRs, mediate the activity-dependent stimulation of molecular layer astrocytes.

During the above experiments, we noticed that about 25% of the astrocytes underwent irregular $[Ca^{2+}]_i$ transients and oscillations even without stimulating the perforant path afferents. We studied this subpopulation in three slices (**Fig. 5g**). In 11 out of 24 such cells, TTX blocked the Ca^{2+} activity, reducing the mean frequency (0.010 ± 0.003 Hz) and amplitude (0.099 ± 0.090 $\Delta F/F_0$) of the events by 90% and 88%, respectively. Application of A3P5PS after washout of the toxin and recovery of the basal activity again inhibited the Ca^{2+} events in the same 11 cells (frequency, –50%; amplitude, –45%). Therefore, both evoked neuronal activity and basal activity endogenously present in the slices activate P2Y1R-dependent signaling in subpopulations of molecular layer astrocytes.

Astrocytic P2Y1R stimulation induces synaptic potentiation

Because P2Y1R stimulation triggers glutamate exocytosis from astrocytes[7], we tested whether activation of these receptors affects synaptic activity in granule cells in a way similar to that observed on electrical stimulation of the astrocytes (**Fig. 1**). At first we studied sEPSC activity (**Fig. 6a**). Application of the P2Y1R agonist 2-methylthioadenosine-5′-diphosphate[23] (2MeSADP) significantly enhanced sEPSC frequency in five out of six patched granule cells (from 1.34 ± 0.22 Hz to 1.78 ± 0.21 Hz; $P < 0.05$) without changing sEPSC amplitude (control, 13.21 ± 1.32 pA; 2MeSADP, 14.25 ± 1.31 pA). The effect of 2MeSADP was abolished in the presence of the NMDAR antagonist ifenprodil. Moreover, ifenprodil *per se* reduced the basal frequency (not amplitude) of sEPSCs (frequency: control, 1.26 ± 0.17 Hz; ifenprodil, 1.02 ± 0.16 Hz, $P < 0.05$ versus control; 2MeSADP + ifenprodil, 1.06 ± 0.18 Hz, $P < 0.01$ versus 2MeSADP; amplitude: control, 14.37 ± 0.55 pA; ifenprodil, 14.68 ± 0.47 pA; 2MeSADP + ifenprodil, 14.33 ± 0.57 pA; $n = 5$). Similar to ifenprodil, the P2Y1R antagonist A3P5PS selectively reduced sEPSC frequency in five out of six patched granule cells (from 1.31 ± 0.19 Hz to 0.68 ± 0.16 Hz, $P < 0.01$; sEPSC amplitude: control, 12.41 ± 1.66 pA; A3P5PS, 12.12 ± 1.35 pA). These data demonstrate that P2Y1R stimulation potentiates sEPSC activity in granule cells via activation of downstream NR2B-containing NMDARs. They also show that a component of basal sEPSC activity in granule cells is P2Y1R dependent (see **Supplementary Note**).

Having shown that such activity stimulates astrocytic P2Y1Rs, we hypothesize the existence of an intrinsic synaptic control via the astrocytes. To verify this hypothesis, we recorded simultaneously Ca^{2+} signals in astrocytes and synaptic activity in granule cells. In

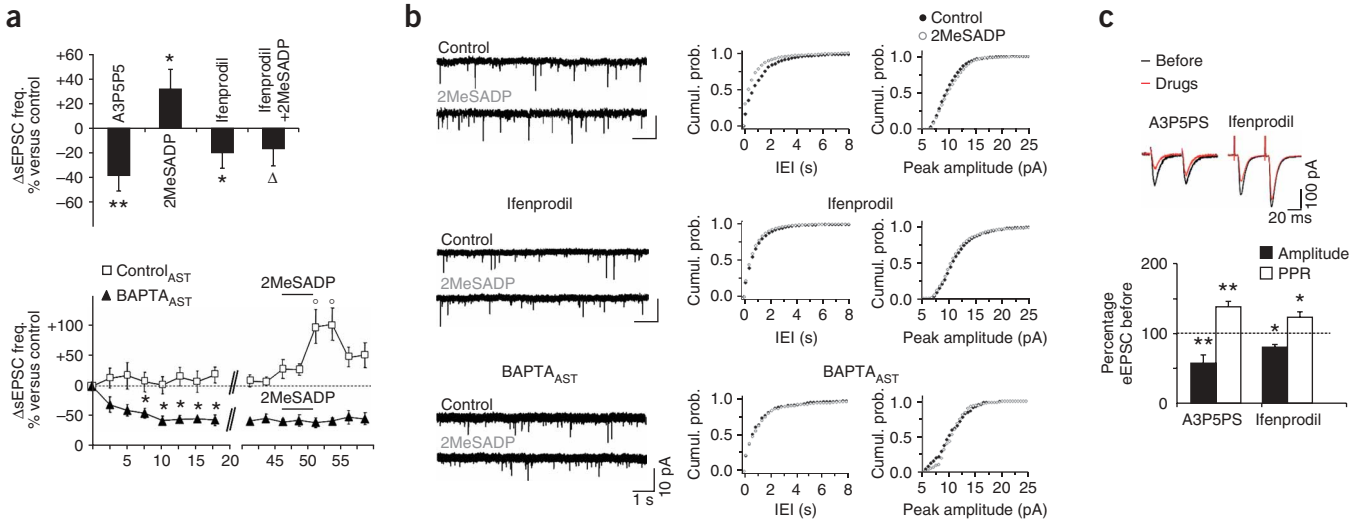

Figure 6 Astrocyte P2Y1R-dependent potentiation of excitatory transmission in granule cells via NR2B-containing NMDARs. (**a**) Top, sEPSC frequency changes (percent versus control) in granule cells induced by 100 μM A3P5PS, 10 μM 2MeSADP, 3 μM ifenprodil or 10 μM 2MeSADP and 3 μM ifenprodil. $^{*}P < 0.05$; $^{**}P < 0.01$ versus control; $^{\Delta}P < 0.05$ versus 2MeSADP, one-way ANOVA and Scheffé test. Bottom, basal sEPSC frequency in granule cells and response to 2MeSADP in double-patch experiments where we did ($BAPTA_{AST}$) or did not ($control_{AST}$) introduce 40 mM BAPTA in the astrocyte. Data: percentage change versus values before patching the astrocyte. $^{*}P < 0.05$ versus $control_{AST}$, one-way ANOVA; $^{\circ}P < 0.05$ versus last bin before 2MeSADP, two-way ANOVA. (**b**) Left, representative mEPSC traces comparing 2MeSDAP effect in the following conditions: control, with ifenprodil (3 μM) and with BAPTA (40 mM) in the astrocyte. Right, corresponding cumulative probability plots for IEI (bin, 0.25 s) and peak amplitude (bin, 0.5 pA). 2MeSADP selectively modifies IEI in the control condition (KS test, $P < 0.001$). (**c**) Top, paired-pulse eEPSC responses to perforant path stimulation before (black traces) and during A3P5PS (20–100 μM) or ifenprodil (3 μM) application (red traces). Bottom, amplitude of the first eEPSC of a paired-pulse (black histograms) and PPR (white histograms) after drug application (percentage of values before drug application). Absolute values (eEPSC amplitude (pA): before A3P5PS, –174 ± 24; A3P5PS, –88 ± 16; before ifenprodil, –242 ± 49; ifenprodil, –194 ± 37; PPR: before A3P5PS, 1.00 ± 0.1; A3P5PS, 1.34 ± 0.18; before ifenprodil, 0.99 ± 0.6; ifenprodil, 1.09 ± 0.7), $^{*}P < 0.05$ and $^{**}P < 0.01$ versus before, paired *t*-test.

four out of four experiments, a 5-s-long train of stimuli (100–300 μA, 200 μs, 30 Hz) to the perforant path increased in parallel $[Ca^{2+}]_i$ in astrocytes and sEPSC frequency in granule cells. A3P5PS significantly reduced both responses ($\Delta F/F_0$: –30 ± 4%, $n = 48$ cells in four slices; ΔsEPSC frequency: –35 ± 18, $n = 4$ granule cells in the same four slices). To directly show that Ca^{2+} signaling in astrocytes mediates the P2Y1R-dependent component of sEPSC activity, we performed experiments on astrocyte-granule cell pairs in which we introduced the Ca^{2+} chelator 1,2-bis(2-aminophenoxy)ethane-*N*,*N*,*N*′,*N*′-tetraacetic acid (BAPTA) selectively into the astrocyte while we simultaneously recorded sEPSCs in the granule cell (**Fig. 6a**, bottom). Within 10–15 min, BAPTA diffused from the patched astrocyte to hundreds of gap junction–connected astrocytes, as verified with the fluorescent analog Oregon Green 488 BAPTA-1 cell impermeant[24] (OGB, **Supplementary Fig. 6** online). In parallel, the frequency of sEPSCs in the granule cell decreased progressively, until it reached a stably reduced level. In this situation, the stimulatory effect of 2MeSADP was abolished (five out of five cell pairs). Because repeating the experiment without BAPTA in the astrocyte neither caused reduction in baseline sEPSC frequency nor prevented 2MeSADP-induced stimulation ($n = 5$), we conclude that $[Ca^{2+}]_i$ elevation in astrocytes is required for the P2Y1R-dependent control of sEPSC activity in granule cells.

We then performed analogous experiments in the presence of TTX to study mEPSC activity in isolation. 2MeSADP increased the frequency of the miniature events in eight out of ten patched granule cells (from 0.74 ± 0.28 Hz to 1.03 ± 0.18 Hz, $P < 0.01$), but did not modify their amplitude and kinetics (control: amplitude, 10.64 ± 1.27 pA; rise time, 1.97 ± 0.89 ms; decay time, 5.24 ± 0.63 ms; 2MeSADP: amplitude, 10.35 ± 1.12 pA; rise time, 1.90 ± 0.20 ms; decay time, 5.27 ± 0.54 ms; **Fig. 6b**). The effect of 2MeSADP was abolished in the presence of ifenprodil ($n = 8$; ifenprodil: mEPSC frequency, 1.01 ± 0.20 Hz; amplitude, 11.93 ± 0.47 pA; ifenprodil + 2MeSADP: frequency, 1.12 ± 0.17 Hz; amplitude, 11.32 ± 0.76 pA) or on intracellular dialysis of BAPTA into the astrocytes (same protocol as above; $n = 4$; $BAPTA_{AST}$: mEPSC frequency, 0.81 ± 0.12 Hz; amplitude, 11.04 ± 0.21 pA; $BAPTA_{AST}$ + 2MeSADP: frequency, 0.71 ± 0.16 Hz; amplitude, 10.8 ± 0.32 pA). These data strongly suggest that activation of astrocytic P2Y1Rs and downstream Ca^{2+} signaling enhances the synaptic input to granule cells via a presynaptic mechanism mediated by NR2B-containing NMDARs.

Finally, we checked whether P2Y1R-dependent signaling contributes to the overall strength of synaptic connectivity during evoked transmission at perforant path-granule cell synapses (**Fig. 6c**). Indeed, blocking P2Y1Rs with A3P5PS ($n = 6$) caused a reduction of the amplitude of eEPSCs. Blocking NR2B-containing receptors with ifenprodil produced an analogous effect ($n = 10$). In both cases, the inhibitory effect was accompanied by a change in the PPR of the eEPSC responses, consistent with the involvement of a presynaptic mechanism.

DISCUSSION

Synaptic potentiation via astrocytic glutamate exocytosis

The present study outlines a newly described astrocyte-mediated mechanism controlling the probability of transmitter release at the synapse and the strength of synaptic connectivity. Excitatory synaptic transmission at synapses on dentate granule cells is reinforced by activity-dependent stimulation of purinergic P2Y1Rs on dentate molecular layer astrocytes and ensuing Ca^{2+}-dependent exocytosis of glutamate that activates presynaptic NR2B-containing NMDARs. By this mechanism, astrocytes participate in synaptic tuning in circuits involved in cognitive processing and the control of limbic system excitability.

The astrocyte mechanism is blocked by $TeNT_{LC}$ selectively perfused into astrocytes, but not by a single-amino-acid mutant of the toxin that has lost the capacity to prevent SNARE-dependent vesicle fusion[17,25]. This observation provides strong evidence for the exocytotic nature of the astrocytic input to synapses. It also represents the first functional confirmation of a communication in brain tissue via exocytosis of astrocytic transmitter. Previous work had identified the presence of SLMVs containing the machinery for storing and releasing glutamate in the perisynaptic processes of hippocampal astrocytes *in situ*[6,9,26]. Because such astrocytic SLMVs contain glutamate in a concentration similar to that of synaptic vesicles of adjacent excitatory nerve terminals (L.H.B., A.V. and V.G., unpublished data), it is very likely that glutamate itself is the transmitter exocytosed from astrocytic processes *in vivo*. We cannot, however, rule out the possibility that additional agents, such as the NMDA coagonist D-serine[27], are released together with glutamate and contribute to the described effects on synaptic activity.

A role for presynaptic NR2B-containing NMDARs

The astrocyte transmitter acts via stimulation of ifenprodil-sensitive NMDARs. Our results strongly suggest that such NR2B-containing receptors have a presynaptic localization. First, synaptic changes induced by stimulating or inhibiting the astrocyte pathway, notably selective variations in mEPSC frequency, are consistent with a presynaptic effect on the probability of transmitter release. Second, the functional data are supported by the direct ultrastructural demonstration that NR2B subunits are abundantly present in membranes of nerve terminals synapsing onto granule cell spines and facing the astrocytes. Our immunogold results do not strictly rule out the notion that glutamate exocytosed from astrocytic processes may also reach and activate extrasynaptic dendritic NR2B-containing receptors on granule cells[28]. However, as these are less numerous and less frequently positioned close to astrocytic SLMVs than are presynaptic NR2B-containing receptors (see below), they are expected to have a lesser impact. This is consistent with the fact that astrocyte-evoked synaptic changes in granule cells were not accompanied by SICs, the characteristic ifenprodil-sensitive current events described[18,19] in CA1 pyramidal neurons and attributed to activation of extrasynaptic dendritic NMDARs by astrocyte-released glutamate. Further evidence against a localization of relevant NR2B receptors in granule cells comes from the experiments in which we blocked granule cell NMDARs by internal perfusion of MK-801 without affecting the NMDA-induced increase in mEPSCs. These observations agree with previous data[28] which indicated that synaptic NMDARs in granule cells contain NR2A or, possibly, NR2A-NR2B combinations, poorly inhibited by ifenprodil[29], whereas ifenprodil-sensitive NR2B-containing NMDARs are most likely presynaptic.

The existence of presynaptic NMDARs controlling transmitter release at the synapse has been reported in several brain regions[29]. This is, however, the first time that an astrocyte transmitter has been identified as the stimulus for their activation. Notably, such activation occurs in the presence of TTX and a physiological extracellular Mg^{2+} concentration, and is replicated by simple application of NMDA. This could be explained by an association of NR2B in the presynaptic membrane with other NMDAR subunits less sensitive to Mg^{2+} block. Moreover, the high input resistance of nerve terminals could favor relief of the Mg^{2+} block in response to even very small excitatory currents. It should be noted that activation of NMDARs by NMDA in Mg^{2+}-containing medium has already been reported[18,30,31], including for presynaptic NMDARs[32].

Structural basis of astrocyte-presynapse communication

Our ultrastructural analysis highlights a correlated distribution of glutamatergic microvesicles in astrocytic processes and extrasynaptic NMDARs in excitatory nerve terminals synapsing on granule cell spines. The distance separating NR2B subunits in nerve terminals from SLMVs in surrounding astrocytic processes is in the majority of cases similar to that separating postsynaptic receptors from 'readily releasable' synaptic vesicles at the active zone of nerve terminals[33].

The presence of NR2B-containing NMDARs on extrasynaptic terminal membranes in direct reach of glutamate released from astrocytic vesicles suggests a focal communication where the interaction between astrocytic transmitter and terminal NMDARs may occur with a spatial precision similar to that observed at neuronal synapses. Together with the evidence of focal communication in the opposite direction, from ectopic exocytotic release sites in nerve terminals to Bergmann glial cells[34], these data challenge the general view that communication between neurons and astrocytes is governed by diffusion rules only[35].

P2Y1R-dependent stimulation of excitatory transmission

Astrocyte-mediated potentiation of excitatory transmission in dentate granule cells occurs through a previously unknown action of purinergic P2Y1Rs. Our results indicate that P2Y1Rs in molecular layer astrocytes are stimulated by ATP released as result of perforant path activity. We have not established the source of ATP: the nucleotide could be released together with glutamate from the afferent fibers themselves[36] or from astrocytes stimulated by synaptic glutamate[37]. Activation of astrocytic P2Y1Rs results in Ca^{2+} release from the internal stores and glutamate exocytosis (see ref. 7 for corroborating evidence). Coupling between P2Y1R signaling and glutamate exocytosis could be characteristic of astrocytes, as P2Y1R stimulation in neuronal preparations, including hippocampal synaptosomes, does not induce glutamate release[7].

P2Y1R-dependent stimulation of excitatory synaptic transmission in granule cells is at variance with several studies reporting an inhibitory effect of astrocytic purinergic signaling in the hippocampus. The latter generally depends on rapid conversion of ATP to adenosine via endonucleotidases, with ensuing activation of adenosine receptors which depress transmitter release[37–40]. Our findings, however, together with analogous observations in the CA1 region of the hippocampus[12], demonstrate that ATP has actions of its own, mediated by P2Y1Rs. The structural-functional relations governing purinergic signaling in specific circuits, for example the reciprocal locations of ATP receptors and endonucleotidases, most likely represent a critical and still largely unknown factor in determining the type of ATP action. In this respect, it is noteworthy that, in the dentate gyrus, we localized P2Y1Rs almost exclusively in the processes of molecular layer astrocytes surrounding asymmetric (but not symmetric) synapses. It is tempting to speculate that this localization is finalized to a 'tripartite' control of excitatory synaptic transmission involving the astrocytes[41]. Theoretically, such a control could have an important function in regulating the flow of afferent impulses entering the hippocampal network, inasmuch as the stimulation of individual molecular layer astrocytes by active perforant path fibers can potentially affect a large number of granule cells (see **Supplementary Note**). The next challenge will therefore consist of identifying the precise contribution that the astrocyte-dependent synaptic control provides to memory storage processes and to physiological limbic system excitability[42], as well as to their dysfunction in pathological conditions[4] including Alzheimer disease[43,44] and temporal lobe epilepsy[45].

METHODS

Chemicals. Picrotoxin, TBOA and MCPG are from Tocris Cookson, TTX is from Alomone Labs, and dextran 40000–fluorescein, Fluo-4 AM, Fluo-4 pentapotassium salt and OGB are from Molecular Probes–Invitrogen. All other chemicals were from Sigma-Aldrich. $TeNT_{LC}$ and $TeNT_{LCE271A}$ were prepared as described previously[6].

Hemibrain slices. Hemibrain horizontal slices (300–400 μm) containing intact perforant path afferents[46] were obtained from 10–22-d-old Sprague-Dawley male and female rats and maintained in artificial cerebrospinal fluid (ACSF) containing 118 mM NaCl, 2 mM KCl, 1.3 mM $MgCl_2$, 2.5 mM $CaCl_2$, 25 mM $NaHCO_3$, 1.2 mM NaH_2PO4, 10 mM glucose and 0.1 mM picrotoxin, adjusted to pH 7.4 when gassed with 95% O_2 and 5% CO_2.

Patch-clamp recordings. Borosilicate glass pipettes for patching granule cells or astrocytes contained, respectively, 135 mM cesium gluconate, 10 mM HEPES, 2 mM $MgCl_2$, buffered to pH 7.2 with CsOH (resistance, 3–5 MΩ), and 130 mM potassium gluconate, 4 mM NaCl, 5 mM EGTA, 10 mM HEPES, 1 mM $CaCl_2$, 1 mM $MgCl_2$, 0.2 mM sodium GTP and 2 mM sodium ATP, buffered to pH 7.2–7.4 with KOH (resistance, 8–10 MΩ). In some experiments, we added 2 mM MK-801 to the granule cell internal medium; in others 120 nM $TeNT_{LC}$ or $TeNT_{LCE271A}$, or 40 mM BAPTA were added to that of the astrocyte. We performed whole-cell recordings at 33 °C with a multiclamp 700A amplifier and acquired them with pClamp 8.1 (Axon Instruments). In dual recordings, we patched cell pairs consisting of a granule cell at the outer border of the granule cell layer and a molecular layer astrocyte[47] with a cell body interdistance of 50–100 μm. Granule cells and astrocytes were voltage clamped at –65 and –80 mV, respectively. Astrocytes (or neuropil) were stimulated with a train of 50 depolarizing pulses (500 ms; 0.5 Hz) via a Master-8 stimulator (A.M.P.I.; **Supplementary Table 1**). Verifications were made that this protocol does not alter the electrical membrane properties of astrocytes (**Supplementary Fig. 1**). Recordings with unstable baseline or drifting greater than –200 pA were rejected. Paired-pulse EPSC responses (interpulse interval, 50 ms) were evoked in granule cells by stimulating perforant path afferents with an extracellular bipolar electrode (TST33A10KT; WPI; paired 200-μs shocks, 0.033 Hz, intensity adjusted to produce 150–350-pA eEPSC amplitudes).

Current analysis. Transient current events continuously recorded in individual granule cells (sampling interval, 5 kHz) were low-pass filtered (2 kHz) and analyzed (in terms of amplitude, frequency, rise time and decay time) in 60–100-s-long bins using the Mini-Analysis Program 5.1 (Synaptosoft). In astrocyte stimulation experiments, three consecutive bins of events were analyzed, just before, during (AST stim) and immediately after stimulation. In drug application experiments, three nonconsecutive bins were analyzed, just before drug application (control), during its perfusion (drug) and after it had been washed out (washout). In experiments with BAPTA in the astrocyte, up to 24 consecutive 150-s-long bins were analyzed. The template chosen for each current event consisted of a 5-ms baseline, complete rise time and 90% of decay time. Only single-peak events were accepted during subsequent visual control. Forty or more events were averaged for any condition in any experiment. Events were identified as synaptic currents (sEPSC or mEPSC) by setting the event detection threshold at 5 pA and by checking that events had (i) rise times faster than decay times, (ii) rise times greater than 0.4 ms and (iii) decay times greater than 1.5 ms. Events were identified as slow inward currents (SIC) when they had rise times greater than 10 ms and amplitudes greater than 20 pA[19]. Events not fitting the above parameters, either 'false synaptic events' (3%) or 'superimposed, nonsynchronized events' (4%, only in sEPSC recordings), appeared as a constant percentage among the experiments and among conditions in the experiments and were rejected. The presence of only few nonsynchronized events in sEPSC recordings is consistent with previous observations in granule cells[46]. For any tested condition, amplitudes, frequencies, rise and decay times of the recorded events were first averaged in each experiment. The resulting means were averaged between experiments. For statistical analysis, the means of all experiments for one condition were compared with the means of other conditions using ANOVA and Scheffé test for multiple comparisons (Scheffé test) or two-tailed *t*-test. The significance of the shift in cumulative probability distributions of interevent interval (IEI) and amplitude was assessed by pooling together the data of all the experiments for each condition and using the nonparametric Kolmogorov-Smirnov two-sample test (KS test). In experiments on eEPSCs at perforant path–granule cell synapses, we averaged ten consecutive paired-pulse eEPSC responses recorded during a 5-min period. Control responses, taken in the 5 min preceding the test, were compared to responses in the test period. In the absence of a test, traces in the test and control period were identical ($n = 4$). eEPSCs were analyzed with pClamp8.1 software. For all graphs and statistics we used Origin 6.1 (Microcal Software, Inc).

Immunocytochemistry. For NR2B immunocytochemistry, rabbit antibodies to a C-terminal peptide (amino acids 984–1,104; Advanced Immunochemical; final dilution, 1:100–1:200) were tested on immunoblots and produced a single band with an appropriate molecular weight (data not shown). NR2B antibodies from Molecular Probes (final dilution, 1:100) produced a similar staining pattern, but of lower intensity (data not shown). Hippocampal specimens from P14 rats, fixed by transcardiac perfusion (4% formaldehyde and 0.1% glutaraldehyde or 1% formaldehyde and 2.5% glutaraldehyde), were embedded in Lowicryl HM20 or in Durcupan[48]. Ultrathin Lowicryl low-glutaraldehyde sections were treated with the antibodies according to an immunogold method[48,49]. Durcupan high-glutaraldehyde sections were used for morphological analysis. Sections were viewed in a Philips CM 10 electron microscope. Electron micrographs were taken in the dentate molecular layer. Astrocytic processes surrounding asymmetric synapses between nerve terminals and dendritic spines were identified according to ref. 50 and by their concave shape and light appearance. An NR2B gold particle was ascribed to the plasma membrane if the center of the gold particle was within 30 nm of either side of the plasma membrane[49]. The spatial relationship between NR2B gold particles (10 nm) and SLMVs in the astrocytic processes was determined by recording the intercenter distance between the particles and the closest astrocytic vesicle, sorting the distances into bins of 20 nm and analyzing their frequency distributions. The NR2B analyses were performed in two rats.

For P2Y1R immunocytochemistry, fixed hippocampal specimens (4% formaldehyde and 0.5% glutaraldehyde) were processed for double immunofluorescence with polyclonal P2Y1R antibodies[20] (5 μg ml^{-1}) and monoclonal GFAP antibodies (0.5 μg ml^{-1}, Boehringer Mannheim) or for immunoperoxidase cytochemistry as described[20]. The peroxidase sections were embedded in Epon and ultrathin sections were viewed in a Jeol 100-SX electron microscope. Electron micrographs were taken in the dentate molecular layer and perisynaptic astrocytic processes were identified as above.

Imaging experiments. Hemibrain slices, incubated with the Ca^{2+} indicator Fluo-4 AM (5 μM, 45 min, 22–24 °C) in ACSF, were maintained at 37 °C and observed on an Olympus BX51WI microscope (20× water-immersion objective). Endogenous Ca^{2+} responses and responses evoked by trains of stimuli (100–300 μA; 200 μs; 30 Hz; 5s) to perforant path afferents were recorded in Fluo-4–loaded cells in the molecular layer. Synaptic activity was sometimes recorded in parallel. The excitation light beam (488-nm, monochromator, Visichrome, Visitron; controlled by Metafluor software, Universal Imaging) was introduced through the objective by a long-pass filter (Olympus U-N31001); fluorescence emission was collected (cooled CCD camera, CoolSNAP-HQ, Roper Scientific) with a 1-frame per s acquisition rate. In some experiments, Fluo-4–loaded slices were co-incubated with SR101 (1 μM, 15 min, 37 °C) and excited at 488 and 580 nm. In other experiments, astrocytes were whole-cell patched with internal solution containing dextran 40000–fluorescein (120 nM; excitation, 488 nm) or OGB (1–20 mM; excitation, 488 nm). In experiments monitoring astrocyte $[Ca^{2+}]_i$ during trains of depolarizing pulses, the usual internal solution contained membrane-impermeant Fluo-4 pentapotassium salt (50 μM) and differed in EGTA (0.1 mM) and $CaCl_2$ (0.025 mM) concentrations.

Image analysis. $[Ca^{2+}]_i$ variations in windows (18 × 18 μm) containing individual astrocytes were estimated as fluorescence changes over baseline ($\Delta F/F_0$) after background subtraction using MetaFluor and MetaMorph software. For Ca^{2+} transients evoked by perforant path or astrocyte stimulation, we measured peak amplitudes in the absence or presence of drugs; for endogenous Ca^{2+} events (threshold, 5% $\Delta F/F_0$) we measured both peak amplitudes and

frequency during 10-min-long sampling periods. Statistical differences were established by one-way ANOVA and Scheffé method for multiple comparisons.

Note: Supplementary information is available on the Nature Neuroscience website.

ACKNOWLEDGMENTS

We thank A. Pietropoli for initial electrophysiology experiments, T. Ivanova for testing the activity of TeNT in astrocytic membrane fractions, D. Attwell and J. Storm-Mathisen for critical comments to the present manuscript and D. Kullmann, D. Muller and S. Oliet for critical comments to previous versions, helpful discussions and suggestions. This work was supported by grants from the Swiss National Science Foundation (3100A0-100850) and Swiss State Secretariat for Education and Research (00.0553) to A.V. and from the Norwegian Research Council to L.H.B. and V.G.

AUTHOR CONTRIBUTIONS

P.J. conducted most of the electrophysiology experiments and analyses of the electrophysiology data. L.H.B. conducted the immunogold experiments and the analysis of the immunogold data. K.B. conducted the Ca^{2+} imaging experiments and some of the electrophysiology experiments. P.B. supervised the Ca^{2+} imaging experiments and the analysis of the Ca^{2+} imaging data. M.S. conducted part of the analyses of the electrophysiology data. M.D. and C.M. conducted the light and electron microscopy experiments concerning P2Y1R localization. F.T. prepared $TeNT_{LC}$ and $TeNT_{LCE271A}$. V.G. supervised the immunogold experiments as well as the analysis of the immunogold data and participated in writing the manuscript. A.V. supervised the project and wrote the manuscript.

COMPETING INTERESTS STATEMENT

The authors declare that they have no competing financial interests.

Published online at http://www.nature.com/natureneuroscience
Reprints and permissions information is available online at http://npg.nature.com/reprintsandpermissions

1. Parpura, V. *et al.* Glutamate-mediated astrocyte-neuron signalling. *Nature* **369**, 744–747 (1994).
2. Bezzi, P. *et al.* Prostaglandins stimulate calcium-dependent glutamate release in astrocytes. *Nature* **391**, 281–285 (1998).
3. Araque, A., Li, N., Doyle, R.T. & Haydon, P.G. SNARE protein–dependent glutamate release from astrocytes. *J. Neurosci.* **20**, 666–673 (2000).
4. Bezzi, P. *et al.* CXCR4-activated astrocyte glutamate release via TNFα: amplification by microglia triggers neurotoxicity. *Nat. Neurosci.* **4**, 702–710 (2001).
5. Pasti, L., Zonta, M., Pozzan, T., Vicini, S. & Carmignoto, G. Cytosolic calcium oscillations in astrocytes may regulate exocytotic release of glutamate. *J. Neurosci.* **21**, 477–484 (2001).
6. Bezzi, P. *et al.* Astrocytes contain a vesicular compartment that is competent for regulated exocytosis of glutamate. *Nat. Neurosci.* **7**, 613–620 (2004).
7. Domercq, M. *et al.* P2Y1 receptor–evoked glutamate exocytosis from astrocytes: control by TNF alpha and prostaglandins. *J. Biol. Chem.* **281**, 30684–30696 (2006).
8. Crippa, D. *et al.* Synaptobrevin2-expressing vesicles in rat astrocytes: insights into molecular characterization, dynamics and exocytosis. *J. Physiol. (Lond.)* **570**, 567–582 (2006).
9. Zhang, Q. *et al.* Fusion-related release of glutamate from astrocytes. *J. Biol. Chem.* **279**, 12724–12733 (2004).
10. Volterra, A. & Meldolesi, J. Astrocytes, from brain glue to communication elements: the revolution continues. *Nat. Rev. Neurosci.* **6**, 626–640 (2005).
11. Pasti, L., Volterra, A., Pozzan, T. & Carmignoto, G. Intracellular calcium oscillations in astrocytes: a highly plastic, bidirectional form of communication between neurons and astrocytes *in situ*. *J. Neurosci.* **17**, *7817–7830 (1997).*
12. Bowser, D.N. & Khakh, B.S. ATP excites interneurons and astrocytes to increase synaptic inhibition in neuronal networks. *J. Neurosci.* **24**, 8606–8620 (2004).
13. Steinhauser, C., Berger, T., Frotscher, M. & Kettenmann, H. Heterogeneity in the membrane current pattern of identified glial cells in the hippocampal slice. *Eur. J. Neurosci.* **4**, 472–484 (1992).
14. Shimamoto, K. *et al.* DL-threo-β-benzyloxyaspartate, a potent blocker of excitatory amino acid transporters. *Mol. Pharmacol.* **53**, 195–201 (1998).
15. Kang, J., Jiang, L., Goldman, S.A. & Nedergaard, M. Astrocyte-mediated potentiation of inhibitory synaptic transmission. *Nat. Neurosci.* **1**, 683–692 (1998).
16. Schiavo, G. *et al.* Tetanus and botulinum-B neurotoxins block neurotransmitter release by proteolytic cleavage of synaptobrevin. *Nature* **359**, 832–835 (1992).
17. Rossetto, O. *et al.* Active-site mutagenesis of tetanus neurotoxin implicates Tyr-375 and Glu-271 in metalloproteolytic activity. *Toxicon* **39**, 1151–1159 (2001).
18. Fellin, T. *et al.* Neuronal synchrony mediated by astrocytic glutamate through activation of extrasynaptic NMDA receptors. *Neuron* **43**, 729–743 (2004).
19. Fellin, T., Gomez-Gonzalo, M., Gobbo, S., Carmignoto, G. & Haydon, P.G. Astrocytic glutamate is not necessary for the generation of epileptiform neuronal activity in hippocampal slices. *J. Neurosci.* **26**, 9312–9322 (2006).
20. Morán-Jiménez, M.J. & Matute, C. Immunohistochemical localization of the P2Y1 purinergic receptor in neurons and glial cells of the central nervous system. *Brain Res. Mol. Brain Res.* **78**, 50–58 (2000).
21. Nimmerjahn, A., Kirchhoff, F., Kerr, J.N.D. & Helmchen, F. Sulforhodamine 101 as a specific marker of astroglia in the neocortex *in vivo*. *Nat. Methods* **1**, 31–37 (2004).
22. Boyer, J.L., Romero-Avila, T., Schachter, J.B. & Harden, T.K. Identification of competitive antagonists of the P2Y1 receptor. *Mol. Pharmacol.* **50**, 1323–1329 (1996).
23. Von Kügelgen, I. & Wetter, A. Molecular pharmacology of P2Y-receptors. *Naunyn Schmiedebergs Arch. Pharmacol.* **362**, 310–323 (2000).
24. Serrano, A., Haddjeri, N., Lacaille, J.C. & Robitaille, R. GABAergic network activation of glial cells underlies hippocampal heterosynaptic depression. *J. Neurosci.* **26**, 5370–5382 (2006).
25. Jahn, R., Lang, T. & Sudhof, T.C. Membrane fusion. *Cell* **112**, 519–533 (2003).
26. Zhang, Q., Fukuda, M., Van Bockstaele, E., Pascual, O. & Haydon, P.G. Synaptotagmin IV regulates glial glutamate release. *Proc. Natl. Acad. Sci. USA* **101**, 9441–9446 (2004).
27. Panatier, A. *et al.* Glia-derived D-serine controls NMDA receptor activity and synaptic memory. *Cell* **125**, 775–784 (2006).
28. Dalby, N.O. & Mody, I. Activation of NMDA receptors in rat dentate gyrus granule cells by spontaneous and evoked transmitter release. *J. Neurophysiol.* **90**, 786–797 (2003).
29. Cull-Candy, S.G. & Leszkiewicz, D.N. Role of distinct NMDA receptor subtypes at central synapses. *Sci. STKE* **255**, re16 (2004).
30. Karadottir, R., Cavelier, P., Bergersen, L.H. & Attwell, D. NMDA receptors are expressed in oligodendrocytes and activated in ischaemia. *Nature* **438**, 1162–1166 (2005).
31. Parri, H.R., Gould, T.M. & Crunelli, V. Spontaneous astrocytic Ca^{2+} oscillations *in situ* drive NMDAR-mediated neuronal excitation. *Nat. Neurosci.* **4**, 803–812 (2001).
32. Duguid, I.C. & Smart, T.G. Retrograde activation of presynaptic NMDA receptors enhances GABA release at cerebellar interneuron-Purkinje cell synapses. *Nat. Neurosci.* **7**, 525–533 (2004).
33. Gitler, D. *et al.* Different presynaptic roles of synapsins at excitatory and inhibitory synapses. *J. Neurosci.* **24**, 11368–11380 (2004).
34. Matsui, K. & Jahr, C.E. Ectopic release of synaptic vesicles. *Neuron* **40**, 1173–1183 (2003).
35. Rusakov, D.A. & Lehre, K.P. Perisynaptic asymmetry of glia: new insights into glutamate signalling. *Trends Neurosci.* **25**, 492–494 (2002).
36. Mori, M., Heuss, C., Gähwiler, B.H. & Gerber, U. Fast synaptic transmission mediated by P2X receptors in CA3 pyramidal cells of rat hippocampal slice cultures. *J. Physiol. (Lond.)* **535**, 115–123 (2001).
37. Zhang, J.M. *et al.* ATP released by astrocytes mediates glutamatergic activity-dependent heterosynaptic suppression. *Neuron* **40**, 971–982 (2003).
38. Mitchell, J.B., Lupica, C.R. & Dunwiddie, T.V. Activity-dependent release of endogenous adenosine modulates synaptic responses in the rat hippocampus. *J. Neurosci.* **13**, 3439–3447 (1993).
39. Dunwiddie, T.V., Diao, L. & Proctor, W.R. Adenine nucleotides undergo rapid, quantitative conversion to adenosine in the extracellular space in rat hippocampus. *J. Neurosci.* **17**, 7673–7682 (1997).
40. Pascual, O. *et al.* Astrocytic purinergic signaling coordinates synaptic networks. *Science* **310**, 113–116 (2005).
41. Araque, A., Parpura, V., Sanzgiri, R.P. & Haydon, P.G. Tripartite synapses: glia, the unacknowledged partner. *Trends Neurosci.* **22**, 208–215 (1999).
42. Jones, R.S.G. Entorhinal-hippocampal connections: a speculative view of their function. *Trends Neurosci.* **16**, 58–64 (1993).
43. Gomez-Isla, T. *et al.* Profound loss of layer II entorhinal cortex neurons occurs in very mild Alzheimer's disease. *J. Neurosci.* **16**, 4491–4500 (1996).
44. Rossi, D. *et al.* Defective tumor necrosis factor alpha–dependent control of astrocyte glutamate release in a transgenic mouse model of Alzheimer disease. *J. Biol. Chem.* **280**, 42088–42096 (2005).
45. Rutecki, P.A., Grossman, R.G., Armstrong, D. & Irish-Loewen, S. Electrophysiological connections between the hippocampus and entorhinal cortex in patients with complex partial seizures. *J. Neurosurg.* **70**, 667–675 (1989).
46. Staley, K.J. & Mody, I. Integrity of perforant path fibers and the frequency of action potential independent excitatory and inhibitory synaptic events in dentate gyrus granule cells. *Synapse* **9**, 219–224 (1991).
47. Bushong, E.A., Martone, M.E. & Ellisman, M.H. Examination of the relationship between astrocyte morphology and laminar boundaries in the molecular layer of adult dentate gyrus. *J. Comp. Neurol.* **462**, 241–251 (2003).
48. Gundersen, V. *et al.* Synaptic vesicular localization and exocytosis of L-aspartate in excitatory nerve terminals: a quantitative immunogold analysis in rat hippocampus. *J. Neurosci.* **18**, 6059–6070 (1998).
49. Chaudhry, F.A. *et al.* Glutamate transporters in glial plasma membranes: highly differentiated localizations revealed by quantitative ultrastructural immunocytochemistry. *Neuron* **15**, 711–720 (1995).
50. Lehre, K.P. & Danbolt, N.C. The number of glutamate transporter subtype molecules at glutamatergic synapses: chemical and stereological quantification in young adult rat brain. *J. Neurosci.* **18**, 8751–8757 (1998).